Geophys. J. Int. (2001) **145,** 535–549

A theoretical investigation of average *H/V* ratios

Donat Fäh, Fortunat Kind and Domenico Giardini

Swiss Seismological Service, Institut für Geophysik, ETH-Hönggerberg, CH-8093 *Zürich, Switzerland. E-mail: faeh@seismo.ifg.ethz.ch*

Accepted 2000 December 7. Received 2000 December 7; in original form 2000 May 12

SUMMARY

The mode summation method and a finite difference technique are applied to investigate the spectral ratio between the horizontal and vertical components (H/V ratio) of ambient vibrations and to explore the variation of the resonance frequency and the amplitude and shape of polarization as a function of the structure and the source positions. Layered structural models are used by assuming a large number of sources distributed around a receiver, with shallow source depths that are randomly assigned. We identify stable parts of the H/V ratios that are independent of the source distance and are dominated by the ellipticity of the fundamental-mode Rayleigh wave in the frequency band between the fundamental frequency of resonance of the unconsolidated sediments and the first minimum of the average H/V ratio. The ellipticity in this frequency band is determined by the layering of the sediments.

The numerical simulations are compared with observations at a site where the thickness and velocity structure of the unconsolidated sediments are known from *S*-wave and surface wave measurements. Two methods are applied to compute the H/V ratio, the classical method in the frequency domain and a method based on frequency–time analysis that allows us to locate *P–SV* wavelets in the time-series. The main problem in comparing synthetics with observations is the contribution of *SH* waves in the observed H/V ratios. We propose a method to minimize these effects and the effects of the superposition of different incoming *P–SV* waves. An inversion scheme is applied to the stable parts of the observed H/V ratio, based on a genetic algorithm, to retrieve the *S*-wave velocity structure from a single ambient vibration record.

Key words: finite differences, genetic algorithms, microtremors, mode summation, numerical modelling, seismic ambient noise.

INTRODUCTION

In the analysis of local seismic hazard, dynamic ground shaking and permanent ground failure are the two most important effects, at least with respect to buildings and lifelines. Dynamic ground shaking is the important factor for buildings. Ground shaking refers to the amplitude, frequency, composition and duration of the horizontal and vertical components of the vibration of the ground produced by seismic waves arriving at a site. These effects depend largely on the local geological ground conditions. By knowing these conditions, the related hazard can be estimated by means of empirical methods or numerical simulation techniques. Therefore, the investigation of the local ground conditions is of primary interest and should be the first part of any site-specific hazard and risk assessment.

The soil parameters can be obtained from geotechnical or geophysical investigations at the site or in its neighbourhood. They may be obtained through direct, active *in situ* measurements such as *P*- and *S*-wave seismics, surface wave measurements with single stations or arrays, and down-hole and cross-hole techniques, as well as through drillings and subsequent laboratory measurements. Of special interest are passive methods based on ambient noise, or microtremors, due to their low costs. These methods can be applied in urban areas where in general it is not possible to carry out active measurements due to the lack of space for the experimental set-up or the impossibility of using explosive sources.

It is well known that the spectral features and polarization of microtremors exhibit a good correlation with the site geological condition (e.g. Lermo & Chavez-Garcia 1994). Among several proposed microtremor methods, the H/V method (Nakamura 1989) has proven to be one of the most convenient techniques to estimate the fundamental frequency of soft deposits. Extensive use of this method allows a detailed mapping of this frequency within urban areas. If borehole data can be used for calibration, the procedure has the potential to allow estimates of average shear wave velocity of the unconsolidated sediments. The results can also be used to recognize thick layers of seismically soft soils, which are not resolved by borehole data (e.g. Fäh *et al.* 1997).

Generally, the waves associated with microtremors are excited by surface sources such as wind–structure interaction, traffic and vibrations from machines and pumps. Long-period microtremors in the frequency range between 0.05 and 0.8 Hz are often due to sources such as ocean waves. Source effects have an important impact on the H/V ratio because the source location and mechanism determine the amplitude of each mode. Interfaces and lateral heterogeneity cause a transmission of wave energy between different wave types and modes and the distance to the site is important for the frequency- and mode-dependent attenuation. The waves involved in the microtremors are surface waves as well as body waves of P and S type, and observed wavefields are composed of different modes that in general are not separated in time.

One target of our research is the amplitude of the H/V ratio and the factors influencing this amplitude of the polarization. While polarization spectra are a useful tool for estimating the fundamental resonance frequency of soft soils, the ratio is inadequate in estimating ground-motion amplification, especially in deep sedimentary basins (Lachet & Bard 1994; Dravinski *et al.* 1996). Currently only the frequency of the first peak of a polarization curve is used as information about the local site structure, and the influences of various factors such as the source–receiver distance and the sediment–bedrock contrast on the H/V ratio are not well understood. Moreover, there is some disagreement in the scientific community concerning the fundamental-mode surface wave contribution to H/V ratios at the fundamental frequency of resonance of the unconsolidated sediments. Nakamura (2000) in a recent paper maintained his original opinion that H/V ratios in the peak frequency range are not affected by the fundamental-mode Rayleigh wave, allowing a direct comparison with the S-wave transfer function. He explained the peak as being a result of vertically incident SH waves. This contradicts the results of Lachet & Bard (1994), who suggested that the peak can be explained with the fundamental-mode Rayleigh wave.

In this work we show, for a well-investigated site, that much information is contained in the shape of the polarization curve and that it can be extracted with appropriate methods. Two independent numerical simulation techniques are applied to the test-site structure to model ambient vibrations and by comparison with measurements at the site we draw conclusions about the properties of the H/V ratios as well as about the local structure. The first numerical technique is the mode summation method, which allows investigation of H/V ratios for well-defined sources and source–receiver distances. With modal summation, H/V ratios are directly computed in the frequency domain. The second technique is a time-domain finite difference (FD) method for which sources are not treated separately and H/V ratios are computed from the time-domain signals.

TEST SITE AND 1-D STRUCTURAL INTERPRETATION

Our test site is a highway underpass construction in northern Switzerland close to the city of Kreuzlingen where a variety of seismic and geotechnical experiments have been conducted (Maurer *et al.* 1999). The principal objective of the investigations was to determine the elastic properties of a series of lacustrine clays within the 0–30 m depth range. The seismic measurements included surface wave measurements, reflection seismics and a seismic surface-to-borehole transmission experiment (Fig. 1). For the surface wave and P-wave reflection measurements, a shotgun was used as the seismic source and the signals were recorded with 30 Hz vertical geophones. The receiver spacing was 1 m and the entire profile length was 40 m and extended from the collar of the borehole. S-wave reflection seismics with horizontal geophones was not successful and did not show a coherent pattern of reflections. For the high-frequency surface-to-borehole experiment, seismic energy was excited at the surface along the 40 m long profile with hammer blows perpendicular to the profile axes. Seismic waves were recorded with a three-component seismometer clamped to the borehole wall at various depths. Shot and receiver spacings were both 1 m. The P- and S-wave onsets were inverted for P- and S-wave velocity depth functions, which were parametrized as a stack of 15 layers with fixed thicknesses. The geotechnical measurements included standard triaxial tests of undisturbed borehole samples. The measurements provided only estimates of the shear modules in the small strain domain $\varepsilon < 10^{-3}$ due to the inherent limitations of the standard triaxial devices at small strains (Maurer *et al.* 1999). Adjacent to the borehole, piezo-cone penetrometer testing was used to delineate vertical changes of the soils.

The resulting P- and S-wave velocity structure of the experiment is given in Fig. 2(a) in black. The uppermost 15 m consists mainly of normally consolidated lacustrine clays. Silty sands with gravel inclusions are found between 15 and 22 m. Between 22 and 25 m the lacustrine clay units reappear. At about 25 m depth a moraine layer is found, which consists of coarse sands and gravel. The details of the moraine layer and the properties of the bedrock (molasse) at 30 m depth cannot be resolved by the seismic survey. Due to the water saturation of the soils, the P-wave velocity continuously increases from 1290 to 1800 m s^{-1}.

This structure was the basis for our simulations. One commonly used approximation for the interpretation of H/V ratios is based on the assumption of a single soft layer over a half-space showing a strong contrast. Indeed, the lateral variability of unconsolidated sediments is often better accounted for by simplified models than by detailed ones. For this reason we consider not only the detailed structural model but also simplified models. The velocity profiles for the surface layers are given in Fig. 2(a), showing the detailed structure obtained by the geotechnical investigations (Maurer *et al.* 1999) as well as averaged velocity models for the sediments.

A common approach for the simplification of a structure is to form the weighted average of velocities of the layers as follows:

$$\bar{v} = \frac{1}{H}\sum_{i=1}^{n} h_i v_i \qquad \text{with} \qquad H = \sum_{i=1}^{n} h_i \,,$$

where h_i is the layer thickness and v_i is the layer velocity. In this case, the average velocity of the soft sediments is 222 m s^{-1}.

The average velocity can also be computed in a way such that the traveltime in an average model corresponds to the sum of the traveltimes in the single layers,

$$\frac{1}{\bar{v}} = \frac{1}{H}\sum_{i=1}^{n} \frac{h_i}{v_i} \qquad \text{with} \qquad H = \sum_{i=1}^{n} h_i \,.$$

In this case, the average velocity of the soft sediments is 203 m s^{-1}. Traveltime-based average velocities are often considered a more fundamental parameter in site response than are

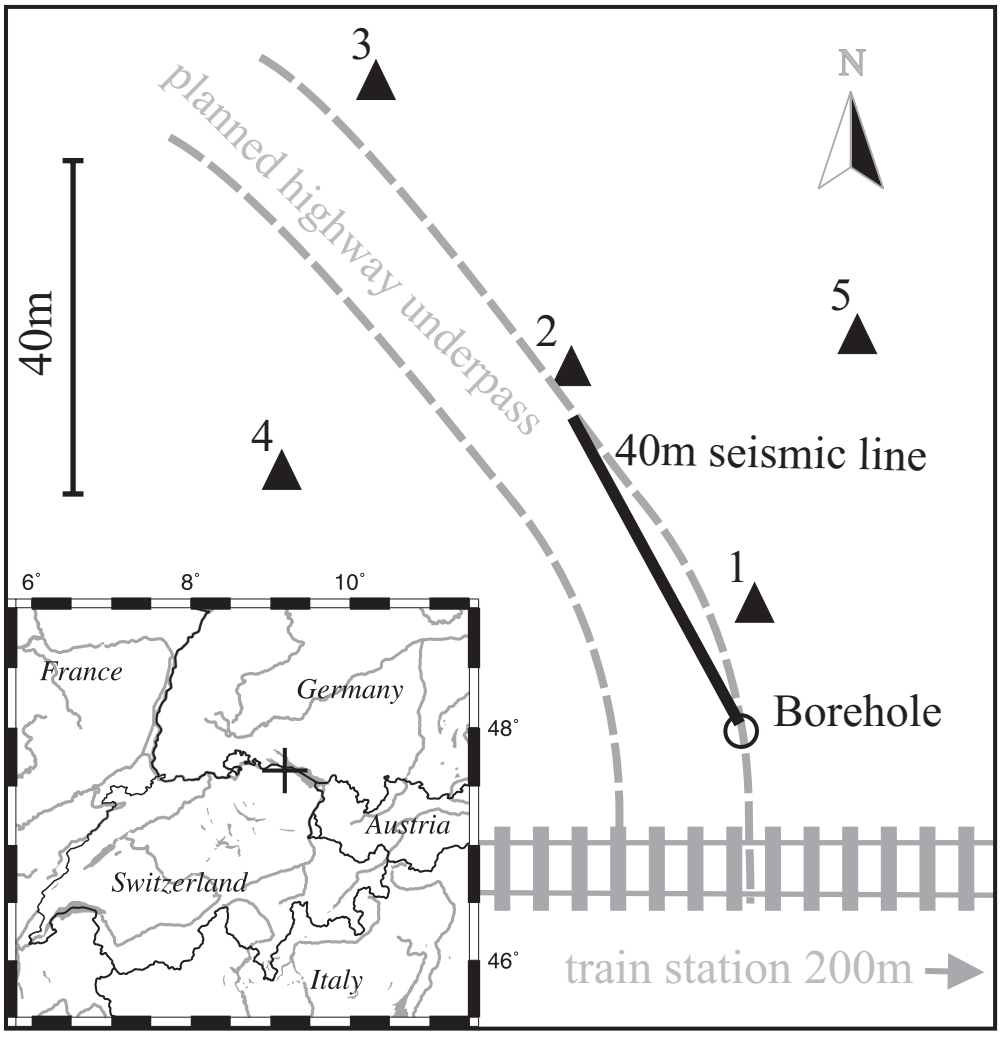

Figure 1. Overview of the test area. The thick black line represents the 40 m seismic line, the circle marks the position of the borehole and the triangles indicate the positions of the noise measurements.

velocity-based estimates (Boore & Brown 1998), because they better reproduce the resonance behaviour of the simplified layer.

One simplified model with two layers ($v_P = 1457$ and 1668 m s^{-1}; $v_S = 164$ and 280 m s^{-1}) and two models with just one layer ($v_P = 1548$ m s^{-1}; $v_S = 203$ and 222 m s^{-1}) were derived. The surface layer is combined with two possible bedrock structures (Fig. 2b). They reflect, at least to some degree, the uncertainty of the velocity model in this depth range. The combinations of bedrock and soil structures result in eight different models that are considered for the investigation of the site observations.

Close to the site, measurements of ambient vibrations have been performed at five different points. Their positions relative to the borehole and to the geophysical experiments are given in Fig. 1. Only the northern part of the geophysical test site was accessible. At each site, the ambient noise has been recorded with a 5 s seismometer for about 15 min and analysed with the classical polarization analysis in the frequency domain, where the polarization is defined as the ratio between the quadratic mean of the Fourier spectra of the horizontal components and the spectrum of the vertical component. The Fourier spectra from individual windows are not smoothed. The polarization spectra are computed for about 45 windows of noise data, each of 20 s length and then averaged for each site. Finally, the average spectral ratio is slightly smoothed. This reduces narrow-band maxima or minima, which can be caused by water pumps working near the sites.

For all five sites, the polarization is plotted in Fig. 3 (grey curves). The peaks of polarization of the ambient-noise wavefield are clearly seen. The fundamental frequencies f_0 measured for the five points are given in Table 1 together with their uncertainty. For the simple model of one single layer over a half-space, the fundamental frequency of resonance is

Table 1. Estimated shear wave velocities from H/V ratios.

Measuring point No.	f_0 (Hz) from H/V ratio	Estimated average v_S (m s^{-1}) and possible range
1	1.74 [1.59–1.93]	209 [191–232]
2	1.73 [1.65–1.89]	208 [198–227]
3	1.75 [1.65–1.86]	210 [198–223]
4	1.88 [1.73–1.95]	226 [208–234]
5	1.82 [1.68–1.93]	218 [202–232]

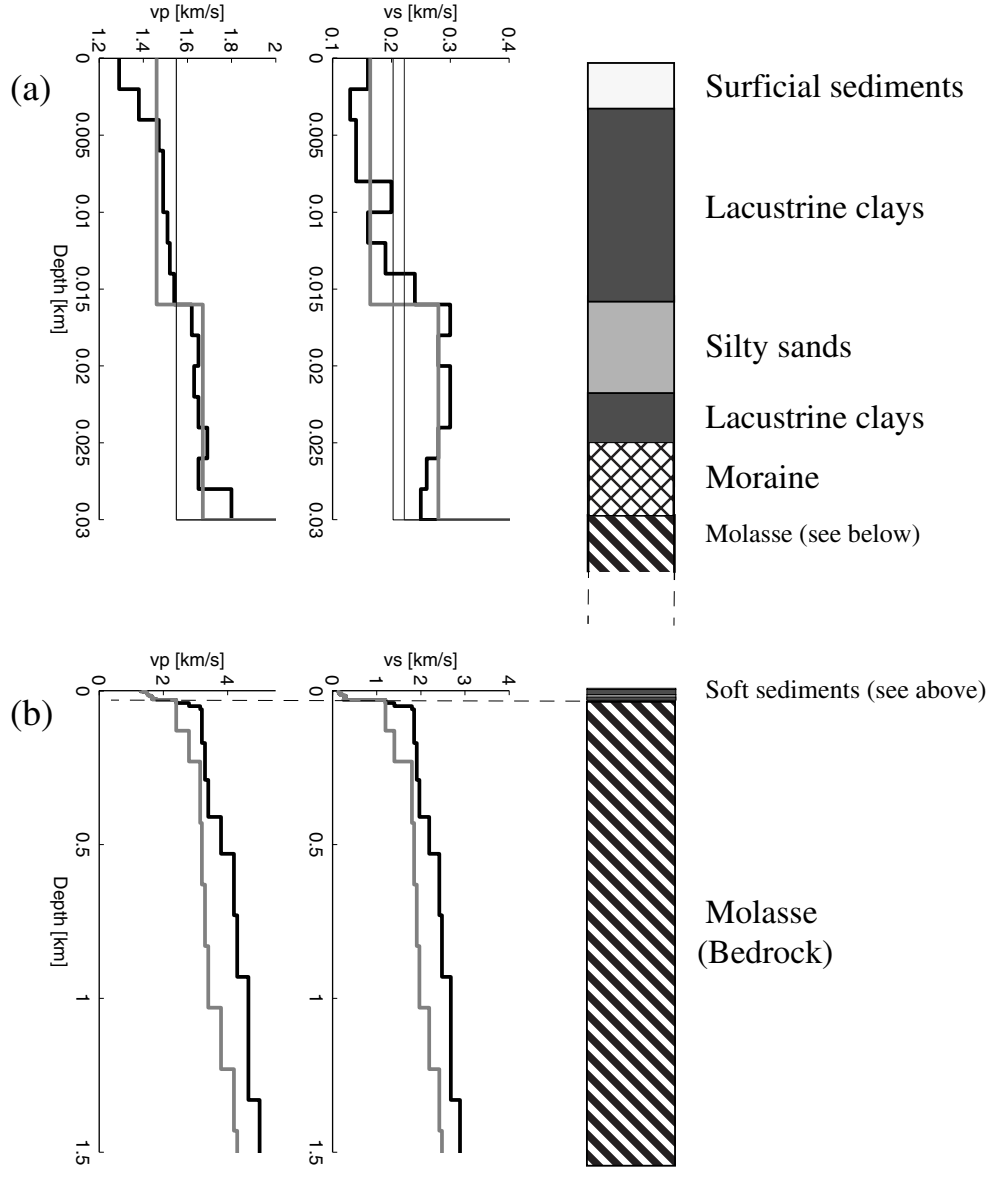

Figure 2. (a) Velocity structure of *P* and *S* waves of the unconsolidated sediments from measurements (Maurer *et al*. 1999) (thick black curve) and the three average models with one and two layers (grey curves). The geological profile was derived from borehole cores. (b) Two structural models for the bedrock that are used for the modelling. This bedrock structure was not resolved by the seismic experiment described in Maurer *et al*.

given by the formula $f_0 = v_S/4h$. By use of this equation and by assuming the depth $h = 30$ m to the bedrock, the average shear wave velocity v_S can be estimated (Table 1). The estimated average velocities vary only slightly between the different measurement points and they are very close to the two averages of 203 and 222 m s^{-1} obtained from the seismic survey (see Fig. 3). This indicates that the assumption of a 1-D structure is valid. There is some variability between the H/V curves in Fig. 3, which reflects the horizontal variability in the structure.

The difference between the seismic survey and ambient vibration measurements is the frequency range of the waves considered. For exploration seismics the analysed energy is centred around 70 Hz, while for the ambient vibrations the range of frequency is between 1 and 10 Hz. In general, anelasticity for such types of sediments is an important effect and this would imply a frequency dependence of the body wave velocity; in the case of constant quality factor Q, this effect is known as body wave dispersion. However, the differences in the velocity estimates between ambient vibrations and the seismic survey is very small and the use of low Q-values is therefore not justified. For this reason, the quality factors of the soils were set to $Q_S = 100$ and $Q_P = 200$ in order to restrict the parameter space in the study and to minimize the influence of the Q-approximation in the two modelling techniques (FD and modal summation). The density of 1800 kg m^{-3} for the soil is estimated from borehole samples (Maurer *et al*. 1999).

SYNTHETIC NOISE

The availability of a thoroughly investigated structure allows the application of numerical simulations in order to study the amplitude and shape of polarization. First, an FD scheme is used to simulate the propagation of *P–SV* waves in horizontally

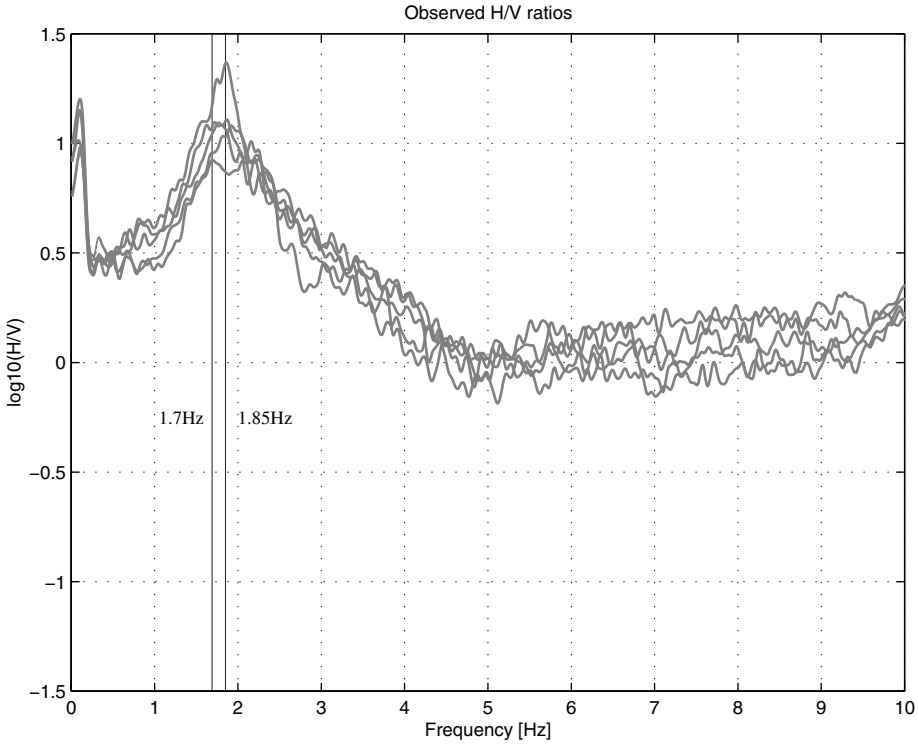

Figure 3. Observed average H/V ratios for the five sites. The fundamental frequencies of resonance of the simplified models with just one layer ($v_S = 203$ and 222 m s^{-1}) are indicated with vertical lines.

layered 2-D models, and second, the modal summation technique is applied. The FD scheme is based on the velocity–stress FD method (Virieux 1986). The algorithm is numerically stable for materials with normal as well as high Poisson's ratios. However, the numerical error increases with decreasing velocities, so it is usually larger near the surfaces of models. Therefore, a fourth-order approximation to the spatial differential operators is used for the upper part of the structural model (Levander 1988). This offers the possibility of reducing the spatial sampling required to model wave propagation accurately. The finite difference operator in time is always of second order. Anelasticity is included by using the rheological model of the generalized Maxwell body (Emmerich & Korn 1987; Fäh 1992). This approximation of the viscoelastic modulus can account for a constant quality factor over the frequency band between 0.1 and 10 Hz. The mesh size in all models is 1×1 m, and the model size is 1400×250 points. With the smallest shear wave velocity of 130 m s^{-1} in the detailed model, at least 13 points per wavelength are achieved with this grid.

Fig. 4 summarizes the procedure for the modelling of synthetic noise. To create the 2-D noise wavefield many different sources are generated in a zone close to the left boundary of the finite difference grid. Their positions in the zone and the source–time functions are generated randomly. In a 1-D structural model, the source characteristics influence the H/V ratio because the excitation of a normal mode depends on the source depth and the source mechanism. Ambient noise should involve mainly surface sources, but lateral heterogeneities that exist in real structures can cause scattering of waves and

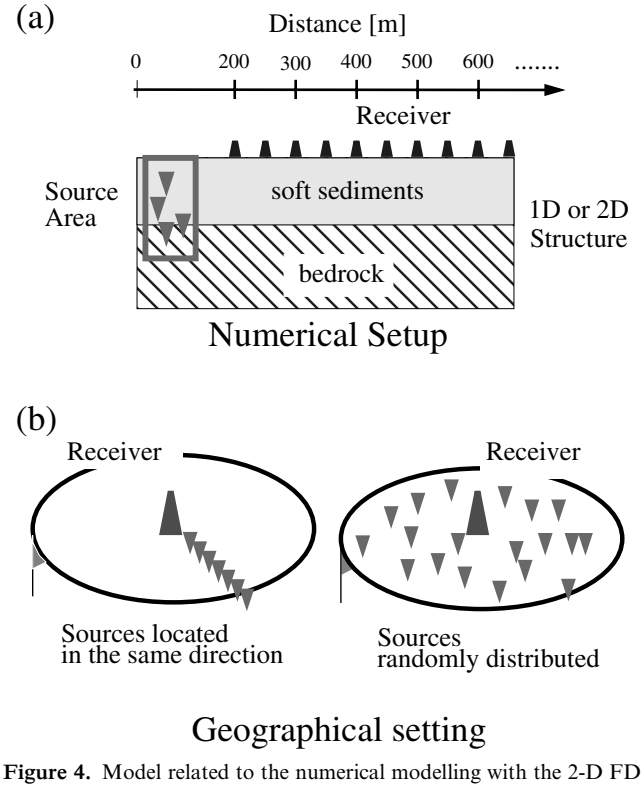

Figure 4. Model related to the numerical modelling with the 2-D FD method and the procedure to obtain noise recordings from sources located in the same direction and from randomly distributed sources.

wave conversions. This is accounted for in the modelling by assuming source locations that can also be located below the layer of unconsolidated sediments. The generated signal is recorded at 50 regularly spaced receivers, the first receiver being located at 200 gridpoints from the left boundary. The computed signals have a duration of 240 s.

To create a more realistic wavefield, several FD synthetics are then combined such that either all sources are assumed to be located in the same direction from the observation point, or they are randomly distributed around the observation point (Fig. 4b). The FD synthetics are summed by assuming a random time-shift for each station and a random amplitude weighting factor. For the case of randomly distributed sources around the observation point, a random azimuth is used for a component rotation of the FD synthetics. The sum of the FD synthetics is used as the actual noise recording. This gives realistic synthetic ambient vibration data for 2-D and 3-D wavefields in a 1-D structure from the finite difference technique.

The second simulation technique used is mode summation. The mathematical theory behind mode summation was established by Knopoff (1964), who gave the solution to the problem of elastic wave propagation in multilayered media in a matrix formulation. By using Knopoff's method, Schwab (1970) and Schwab *et al.* (1984) improved the accuracy of the computed phase velocities by introducing a normalization procedure to control overflow/underflow problems. Panza (1985) and Panza & Suhadolc (1987) then applied the method to the modelling of Rayleigh and *P–SV* synthetics for high frequencies by introducing the concept of the mode follower and the structure minimization procedure. This allowed an efficient computation of the phase velocities for different modes at small frequency intervals with sufficient precision. Florsch *et al.* (1991) applied the same idea to the computation of Love and *SH* waves. For each frequency and mode, the following quantities are necessary to compute synthetic signals: the phase velocity, the phase attenuation, the group velocity, the ellipticity and the eigenfunctions.

The basic input for these computations consists of a layered structure, which in our case is one of the eight models in Fig. 2. Assuming a layered structural model, the microtremor wavefield can be described as the sum of normal modes for the *P–SV* and *SH* parts separately. Inherently, the *SH* part of the wavefield is polarized on the horizontal component of motion. In the *P–SV* case, each mode has its own polarization or ellipticity. As can be seen in Fig. 5, not only the fundamental mode Rayleigh wave but also the higher modes are strongly polarized at the fundamental frequency of resonance of the sediments at about 1.8 Hz. The set of normal modes computed with modal summation is complete for a given phase velocity band (0–4670 m s^{-1}) and frequency band (0.05–10.0 Hz), which allows all body waves and Rayleigh waves within these limits to be modelled. The ellipticity at each frequency is defined as the ratio between the horizontal and vertical displacement eigenfunctions at the free surface, and is therefore basic information for interpreting an observed H/V ratio. The modal summation allows for the generation of signals in a controlled way for an arbitrary combination of modes and can therefore give insight into the physics of the H/V ratio.

When comparing synthetic signals for H/V ratios with observed data there is the problem of the *SH* part of the wavefield. In *P–SV* simulations it is simply absent and as it would contribute to the horizontal part of the H/V ratio, the values from the synthetics are systematically lower. In general, Airy phases are not located at the same frequencies for Rayleigh and Love waves and we might expect a different spectral content for

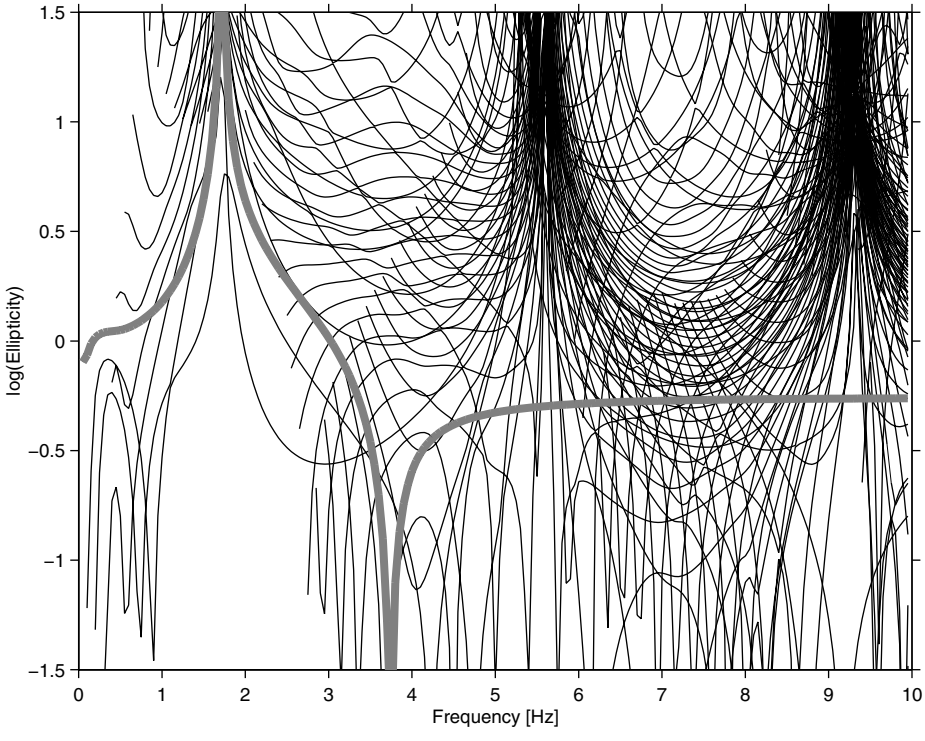

Figure 5. Ellipticity of the fundamental-mode Rayleigh wave (thick grey line) and the higher modes (thin black lines) for a layered structural model with one layer of unconsolidated sediments with $v_S = 222$ m s^{-1} and a thickness of 30 m.

the two wave types. Another difficulty is that source locations and mechanisms of ambient vibrations are unknown, and therefore the *SH*-wave contribution cannot be determined from a single station measurement. This requires some assumptions concerning the spectral content of *SH* waves. A reasonable assumption is that the transverse part of the wavefield has a spectrum and energy content similar to the radial part. This would result in a scaling factor of $\sqrt{2}$ for the synthetic results. However, the information of interest is contained in the *P–SV* part of the wavefield, and the *SH* part blurs the *H/V* ratios. In the next section we develop a new method for computing *H/V* ratios that allows a better detection of the minima in the *H/V* curves.

A NEW TECHNIQUE FOR SPECTRAL *H/V* RATIOS

Although the *P–SV* part and the *SH* part of the wavefield cannot be separated in principle in the recorded microtremor signal, their independence in the propagation through the structure can be used to improve the calculation of the spectral ratio. First, a window of noise data is selected. The basic idea is to identify a wavelet in this window with a strong *P–SV*-wave contribution and take the spectral ratio only for this wavelet. This is done by means of a frequency–time analysis of each of the three components of ambient vibrations. In the frequency–time analysis plot of the vertical component, the most energetic part is identified in time for each frequency and therefore *P–SV* wavelets are located. The polarization or *H/V* ratio of the wavefield is now computed locally in time as the ratio between a maximum spectral value of the horizontal component and the spectral value of the vertical component at the arrival time of the wavelet. The horizontal component of the wavelet may be phase shifted compared to the vertical component, and from the frequency–time analysis we have a time-dependent value for the spectra derived from very short time windows. So as to be sure that the spectral value of the horizontal corresponds to the wavelet on the vertical component, the quadratic mean of both horizontal components is formed. At each frequency the maximum spectral value is selected from the time-dependent spectra within a given time window of the length of one wave period and centred at the arrival time of the main energy on the vertical component.

The polarization spectra with this new technique are computed for the different windows of the noise data and then averaged without any smoothing. In the case of well-separated wavelets this procedure enables us to reduce the effects of *SH* waves. This will be shown first with synthetic data. Fig. 6(a) demonstrates the method for the case of two fundamental-mode Rayleigh wave signals that are excited by two different sources and generated with the modal summation method. The structural model is the average model with one layer (222 m s^{-1}) and the bedrock structure with higher wave velocities. The theoretical polarization of the Rayleigh wave (thick grey line) has one maximum at frequency f_0 (1.8 Hz) and one minimum at about 3.75 Hz. Both extrema can be seen in the classical *H/V* ratio (thin black line) and the new technique (crosses). In frequency bands around f_0 with low energy content of the Rayleigh waves, the classical method works better. For frequency bands with large energy on the vertical component, there is a very good fit between the theoretical *H/V* ratio and the result from the frequency–time analysis. The disagreement at high frequency between the result of the classical method and the theoretical curve is probably due to the low energy in this frequency band.

Random noise is now added to the signals on all three components (Fig. 6b), which accounts for the presence of *SH* waves and therefore describes a more realistic situation. The spectral content of this noise is chosen equal to the spectrum of the horizontal component of the simulated *P–SV* wavefield. While the new method leads to acceptable results, the classical *H/V* ratio is not reliable for the frequencies above 2 Hz. The frequency f_0 in the classical ratio is slightly shifted to smaller values. This experiment shows that as long as the level of unpolarized waves is smaller than the polarized signal, an average over many time windows could improve the results around the minimum *H/V* ratio with the new technique, while for the classical *H/V* ratio it cannot. A special advantage of the new method is the capacity to detect the minimum of the *H/V* ratio even in the presence of uncorrelated noise of strongly excited *SH* waves.

The application of the method to observed noise recordings is shown in Fig. 6(c). There is a larger scatter than for the results obtained from the synthetic data, for both the automatically selected arrival times of the wavelets and the computed *H/V* ratios. This is due to the complexity of the observed ambient vibration wavefield, which is the superposition of *SH* waves and *P–SV* waves arriving at the same time from different directions. The average curves obtained from the classical method based on the Fourier spectra (thin black line) and from the method based on frequency–time analysis (thick grey line) are shifted vertically. This is mostly due to the contribution of *SH*-wave energy in the classical *H/V* ratio.

We now increase the complexity of the synthetic data by applying the FD method to the same one-layer model (v_S=222 m s^{-1}). The signals are combined by assuming that all sources are located in the same direction in one case, and randomly distributed around the receiver in another case. In Fig. 7(a), the two methods to obtain the *H/V* ratio are applied to the synthetic signals. The curves obtained from the classical method based on the Fourier spectra (thin black lines) fit almost perfectly the ellipticity of the fundamental Rayleigh mode (thick grey line), except for the maximum *H/V* value and the frequencies below the fundamental frequency of resonance, f_0. The frequency–time analysis of the same signals leads to lower values (thin grey lines), with the exception of the minimum of the *H/V* curve at about 3.75 Hz, where a good fit is achieved. The reason for the deviation could be constructively interfering *P–SV* waves arriving at the same time on the vertical component, with destructive interference occurring on the horizontal components. In the FD signals, no single mode or wavelet can generally be isolated as demonstrated in Fig. 6, so the deviation from the fundamental mode could also be due to higher modes.

SH random noise is now added to the FD signals on the transverse component of motion (Fig. 7b) with the same spectral content as the simulated radial component. All average *H/V* curves obtained from the FD signals are shifted to higher values. Due to the combination of the two horizontal components with the same frequency content, the horizontal component has an amplitude that is increased by a factor of $\sqrt{2}$. The *H/V* ratios derived with the classical method are therefore shifted by log10($\sqrt{2}$) in the given logarithmic scale when compared to the

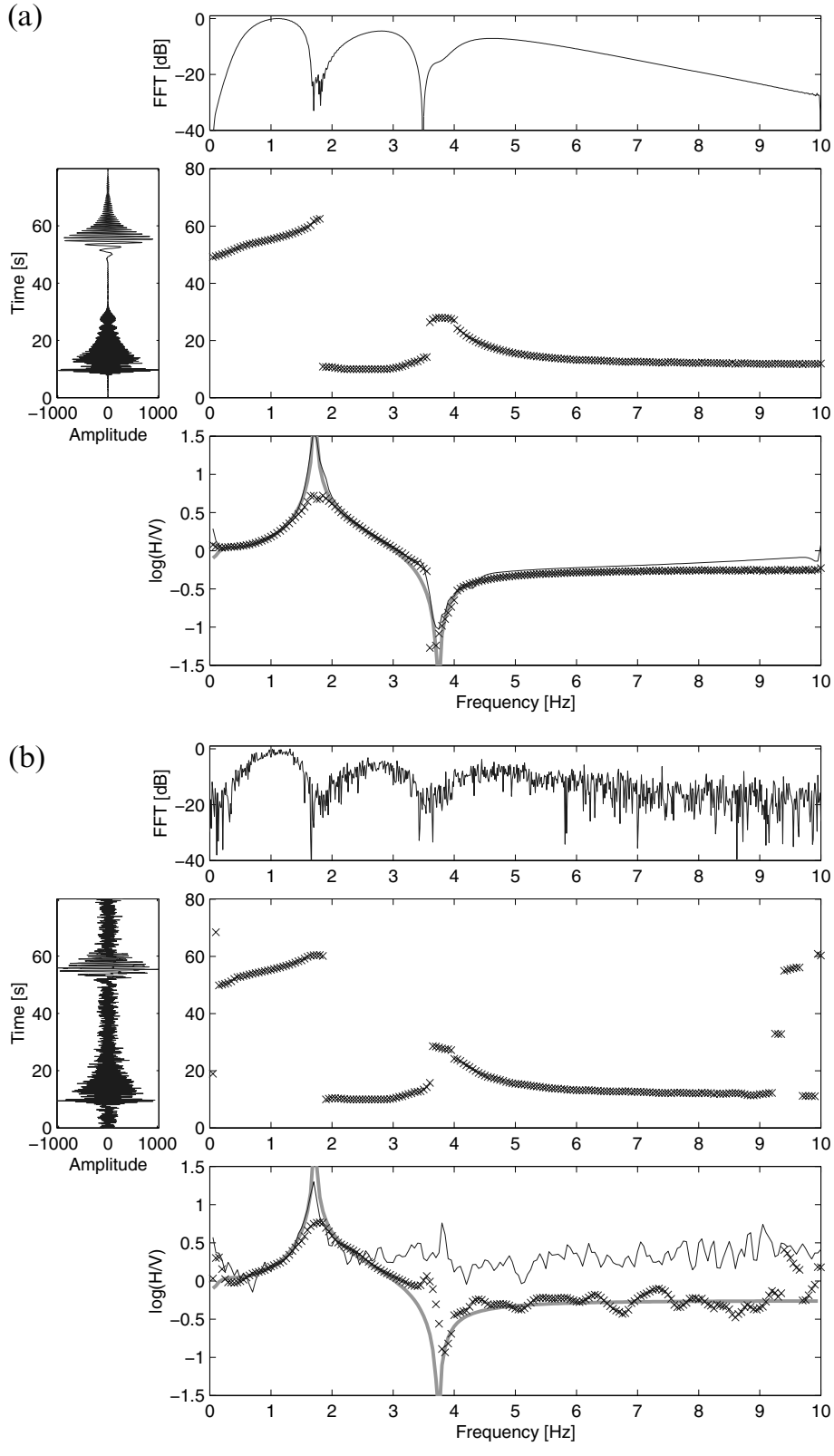

Figure 6. *H*/*V* ratio obtained with the method based on the frequency–time analysis of the three components (a) synthetic data without random noise, (b) synthetic data with random noise added to all components of motion and (c) the analysis of observed noise recordings at observation point 2. The four parts of the figures are the velocity trace of the vertical component of motion (graph on the left), the Fourier spectrum of the vertical component (upper graph), the result of the frequency–time analysis (central graph) showing the arrival time of the most energetic part of the vertical component, and the *H*/*V* ratio computed at this arrival time (crosses). For the synthetic data in (a) and (b), the thick grey line corresponds to the ellipticity of the fundamental-mode Rayleigh wave and the thin black line is the result from the classical polarization analysis in the frequency domain. For the observed noise recordings in (c), the thick grey line corresponds to the average result obtained from the analysis of 10 time windows, and the thin black line is the result from the classical polarization analysis in the frequency domain.

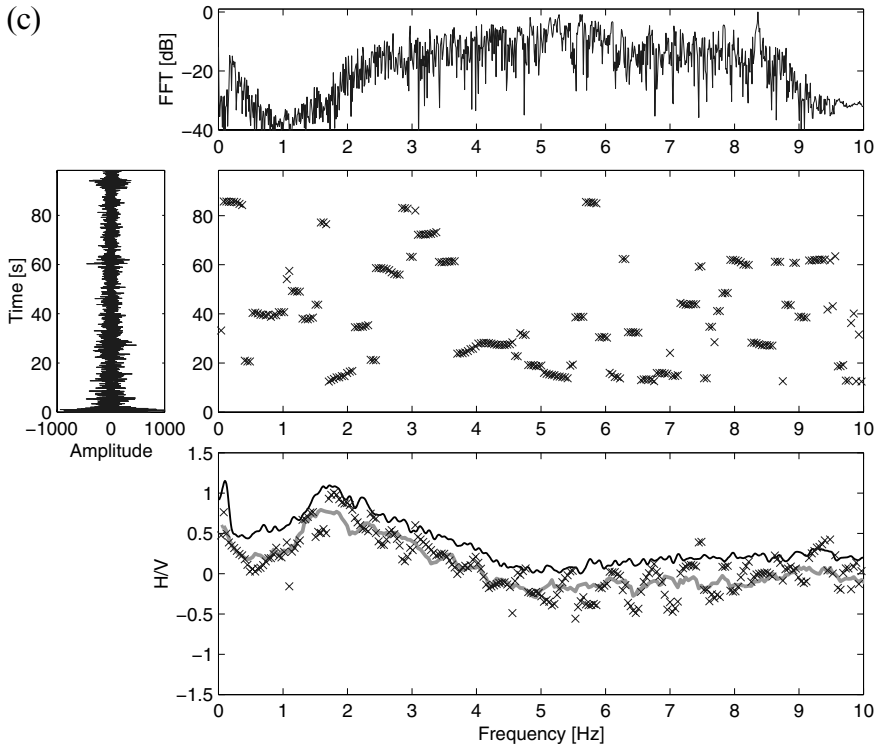

Figure 6. (*Continued.*)

ellipticity curve of the fundamental mode. In the case of added *SH* noise, we conclude that the H/V ratios from the frequency–time analysis identify very well the fundamental Rayleigh mode for the simulated structure in all tested simulations, but do not give the same amplitude near the fundamental peak f_0. The agreement at low frequencies below f_0 is remarkable. These observations are valid for structures with a high velocity contrast between sediments and bedrock, but the situation can differ for low-contrast structures, as we show in the next section.

INVESTIGATION OF THE TEST SITE

We now investigate two important factors influencing the H/V ratios of an ambient vibration wavefield. One is the source–receiver distance and the other is the shear wave velocity contrast between the surface layer and the bedrock. For this purpose we consider *P–SV*-wave polarization calculated from modal summation, which allows the treatment of well-defined source–receiver distance ranges.

To study the influence of the source–receiver distance, a large number of different, randomly distributed sources are assumed in a certain distance range $[x, x+50$ m] and depth range [0 m, 50 m]. 20 distance ranges are treated, namely [50 m, 100 m], [100 m, 150 m], . . . , [1000 m, 1050 m] with 100 different random source mechanisms for each range. For each range, the average H/V ratio is computed from the 100 H/V ratios of the single runs with different sources. The structure is the same as for the FD modelling above. The result is given in Fig. 8(a). Below the frequency f_0 there is a large variability between the average H/V ratios of the different source distance ranges with similar shape of the ratios. In the frequency range between f_0 and 5 Hz, the H/V ratios are all in good agreement with the ellipticity of the fundamental-mode Rayleigh wave. This indicates that this mode can easily be excited for the distance ranges considered and that it dominates the wavefield. Above 5 Hz, there is once again a large scatter between the average H/V ratios of the different distance ranges.

The shear wave velocity contrast between unconsolidated sediments and the bedrock influences strongly the theoretical polarization spectra. For smaller contrasts a dominant amount of energy from higher-mode Rayleigh waves can contribute to the ambient noise in all frequency ranges. To reproduce this effect, we increase the shear wave velocity of the surface layer in our structural model. We want to retain the general shape of the polarization curve, so the depth of the first layer is increased such that the fundamental frequency of resonance would remain the same. For a shear wave velocity of 444 m s^{-1} at 60 m depth, the average H/V ratios for the different distance ranges are still quite well aligned for frequencies between 2.0 and 4.0 Hz (Fig. 8b). However, when the shear wave velocity of the sediments is further increased to 666 m s^{-1} and the depth to 90 m (Fig. 8c), the correspondence between the ellipticity of the fundamental mode and average H/V ratio is completely lost and higher modes dominate the polarization. Moreover, a fundamental frequency of resonance cannot be recognized anymore. This implies that the observed stability of the upper flank of the main peak in the H/V ratios is limited to the case of a strong contrast or in other words to sites where the fundamental Rayleigh mode dominates the wavefield.

For the different distance ranges, the maxima of the H/V ratios are not at the same frequency f_0, even for the example with low shear wave velocities (Fig. 8a). This shows that the fundamental frequency f_0 can only be determined within some uncertainty that is affected by the ellipticity of the excited normal modes and the distance range of the sources. For local site studies with the polarization analysis this should be taken into account to give a measure of the real uncertainty.

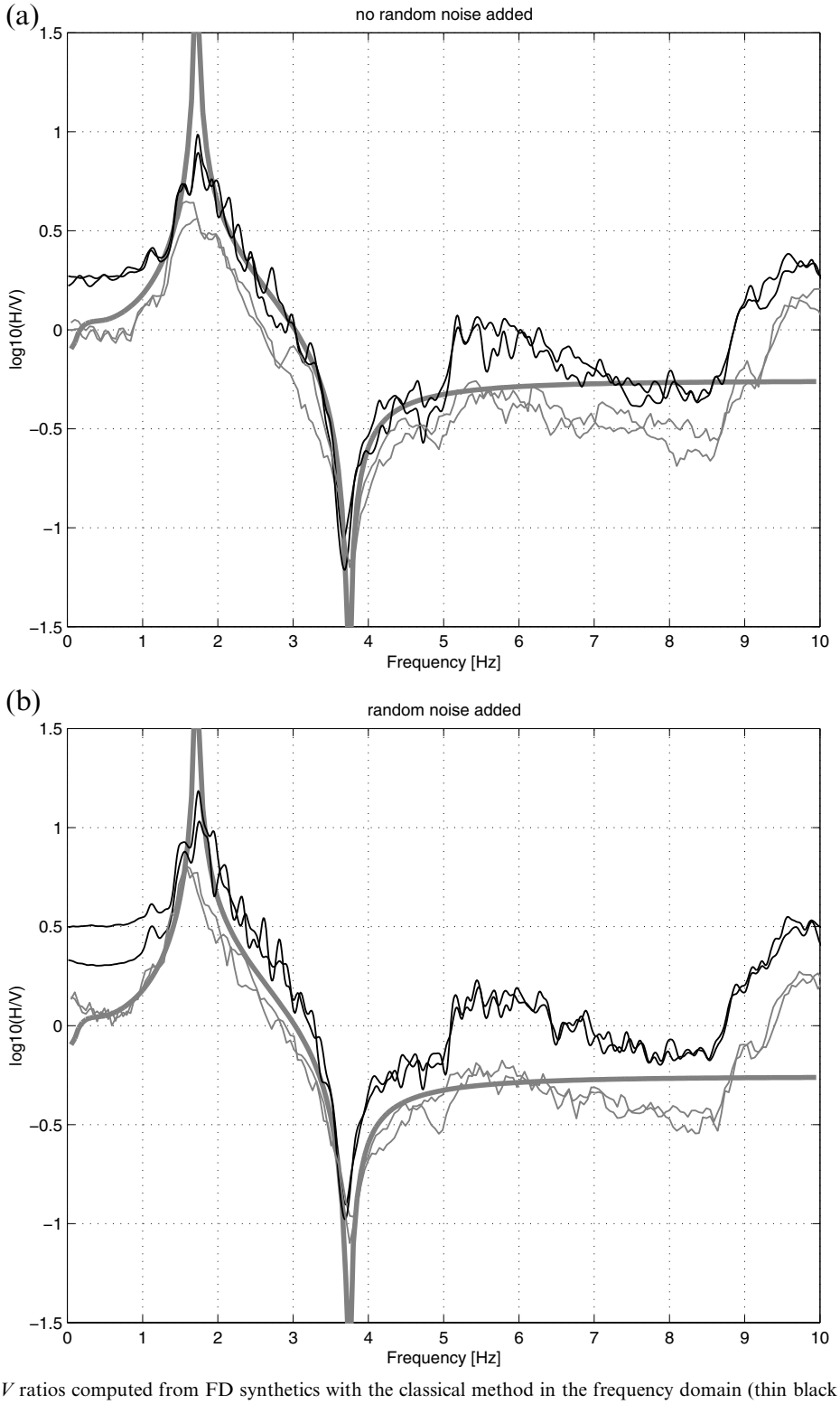

Figure 7. Average H/V ratios computed from FD synthetics with the classical method in the frequency domain (thin black lines) and the method based on frequency–time analysis (thin grey lines). The thick grey line in the background is the ellipticity of the fundamental-mode Rayleigh wave. Two cases are considered: (a) without random noise and (b) with random noise added on the *SH* component of motion.

In a second step, we study the effect of the eight models for the local structure (Fig. 2) on the variation of the H/V ratio. With the FD technique, ambient vibration signals are generated for sources distributed randomly around the receiver. The results from the analysis with the classical H/V method are shown in Fig. 9(a) as thin black curves with the results from the observations in the background as grey curves. Clearly, the synthetic values are systematically lower, which we attribute to the lack of an *SH* part of the wavefield. The first peak is in the range 1.6–1.8 Hz, in good agreement with the observations.

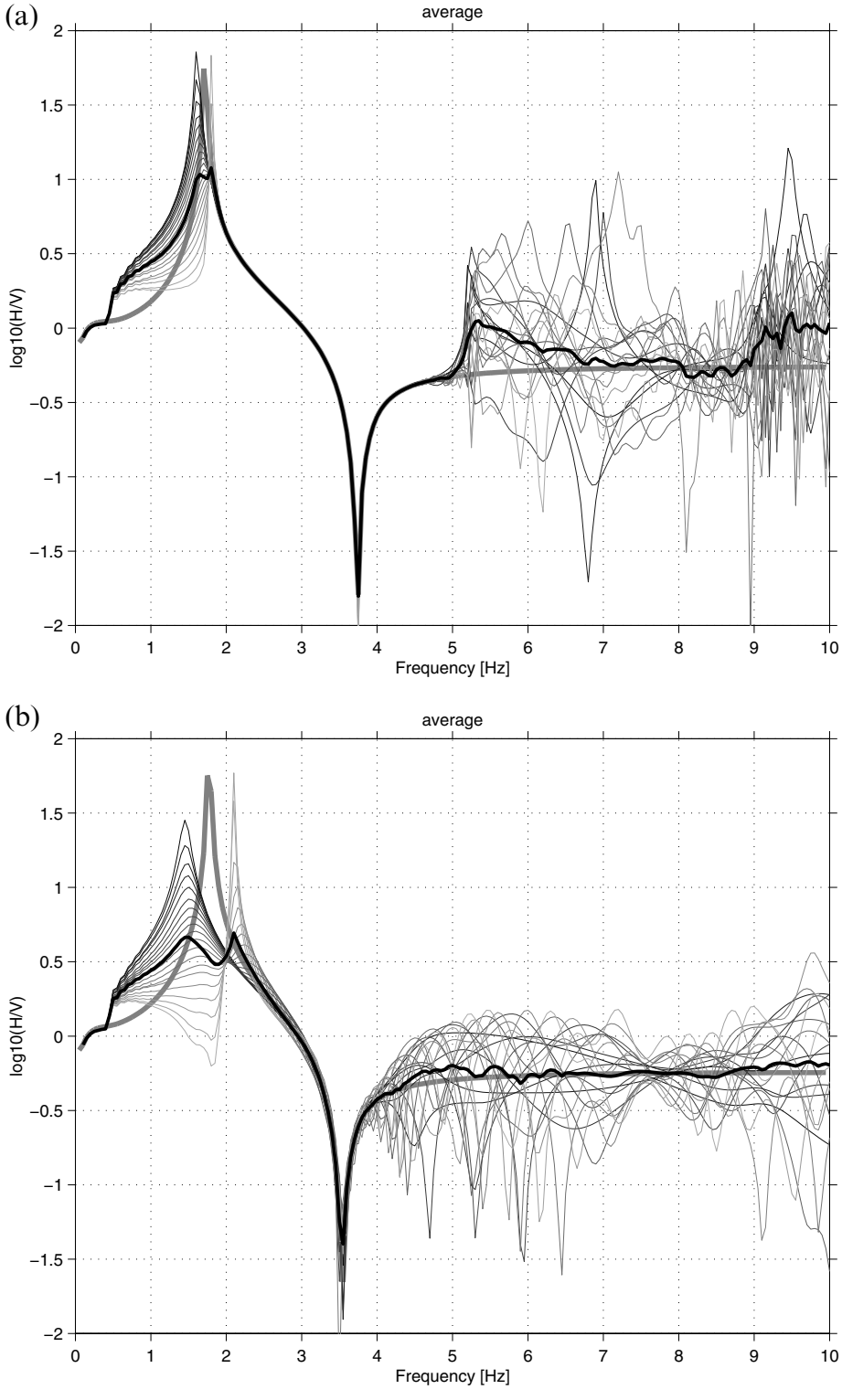

Figure 8. Average H/V ratios assuming different distance ranges for the seismic sources. For each distance range, 100 random sources are taken for the average. For near distances the average H/V ratio is shown as thin black lines and for far distances the curves are grey. The thick black line is the average H/V ratio over all thin curves. The thick grey line in the background is the ellipticity of the fundamental-mode Rayleigh wave. Three cases are considered. The structural models have one sediment layer with (a) a shear wave velocity of 222 m s^{-1} and a thickness of 30 m, (b) a shear wave velocity of 444 m s^{-1} and a thickness of 60 m, and (c) a shear wave velocity of 666 m s^{-1} and a thickness of 90 m.

The amplitudes of these peaks are also similar to the observations, so the simplification of a single layer over a half-space is easily capable of reproducing the first peak in the H/V ratio. The differences between the eight models appear in the minimum of the curve behind the first peak. The sediment layering and velocities are responsible for the position of the minimum following the first peak. The bedrock velocity only slightly affects the amplitude of the H/V ratio at the minimum. Most

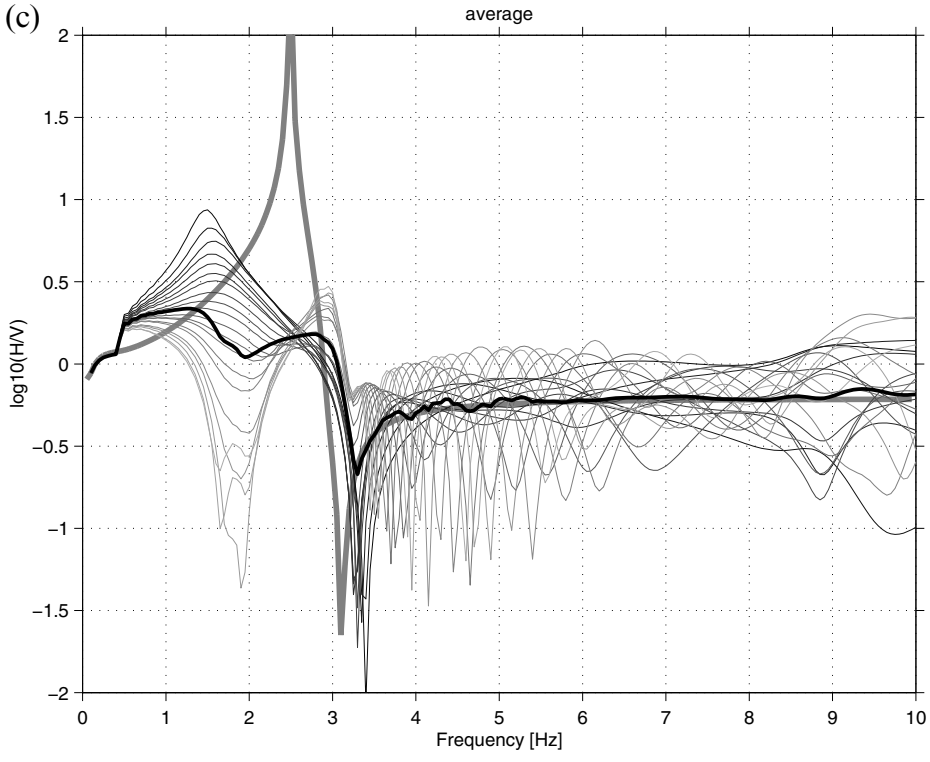

Figure 8. (*Continued.*)

important is the difference between the simplified models and the detailed model, as the minimum is much less pronounced for the detailed structure and the slope of the peak flanks is closest to the observational data. We conclude that the minimum after the peak and the curve segment between peak and minimum depend strongly on the structural parameters of the unconsolidated sediments and cannot be reproduced by a simple 1-D model with one or two layers only.

Next the modal summation method is applied to the same eight models as before and compared to the observations at the test site. The resulting H/V ratios are shown in Fig. 9(b). This time uncorrelated *SH* noise is added to the synthetic signals in the manner discussed above so as to have a better comparison for the actual shape of the peaks. The same observations as for the FD models can be made and the results of the two modelling techniques are comparable. Additionally, the shear wave velocity contrast between bedrock and sediments has an effect on the amplitude around the frequency of resonance f_0. The larger the contrast, the larger the amplitude of the H/V ratio, while the scatter in H/V at the fundamental frequency is considerable. The bedrock does not affect the H/V ratio between the maximum H/V value and the minimum, because fundamental-mode Rayleigh waves that determine the ratio in this frequency band for these models are almost completely trapped in the soft sediments. As expected from the results in Fig. 8, there can be a large scatter in average polarization for frequencies above the frequency of the minimum H/V ratio. As will be shown below, the analysis of the observed ambient vibrations with the frequency–time analysis does not reveal a remarkable minimum of the H/V ratio, and the results are similar to Figs 9 (a) and (b).

The results from the numerical simulation with the eight different models differ significantly from the observed H/V ratios. The largest differences are obtained for the structures with one single layer only. The well-pronounced minima for these structures cannot be seen in the observations because real structures are generally characterized by a velocity increase with depth. Therefore, for the model with realistic layering, results become closer to the observations. A gradient in *S*-wave velocities in the unconsolidated sediments leads to a decrease of the amplitude of the minimum in the average H/V ratio and to a shift of the minimum of the ratio to higher frequencies. A structural model that would reproduce the observations is expected to have a gradient in *S*-wave velocity with slightly different velocities from the structure obtained by the detailed geotechnical investigations.

INVERTING FOR THE STRUCTURE

We have seen that the shape of H/V ratios for the frequency band between the fundamental frequency of resonance and the first minimum depends mostly on the layering in the sediments. With the method based on frequency–time analysis, we could identify the fundamental mode close to the minimum of the average H/V curve. It might therefore be possible to use this information, together with the result from the classical method, to find a structural model for the test site that explains the observed H/V curves. This has been attempted and the result is shown in Fig. 10, with the observed and simulated polarizations in Fig. 10(a) and the structures for comparison in Fig. 10(b). In order to compare directly observed and simulated H/V ratios (classical method), the observed curve is reduced by $\log10(\sqrt{2})$ (thin black line in Fig. 10a) assuming that the spectral content of the *SH* waves is equal to the spectrum of the radial component of the *P–SV* wavefield. The H/V ratio obtained with the

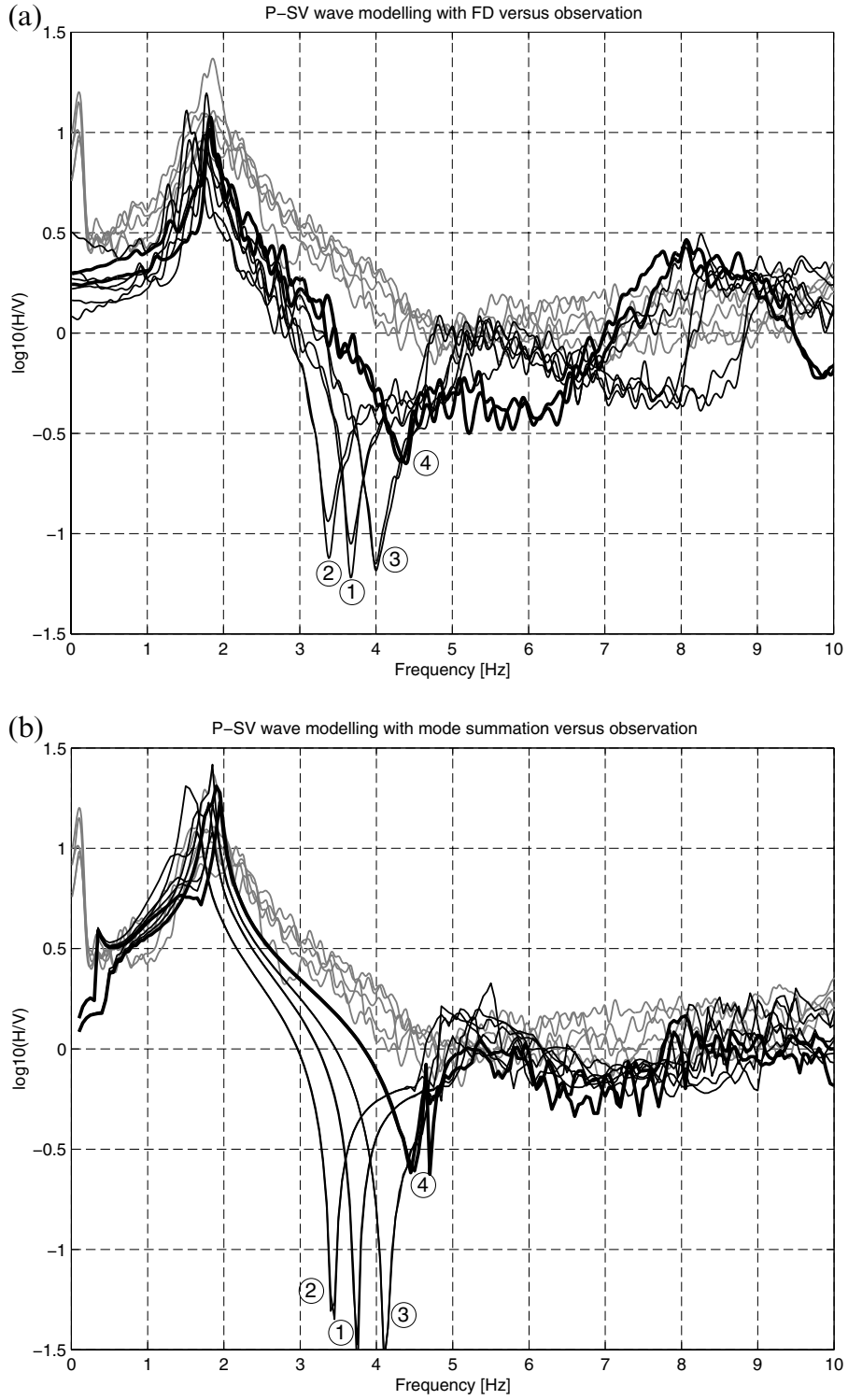

Figure 9. (a) Observed average H/V ratios for the five sites (grey curves) and H/V ratios from synthetic noise (black curves) obtained with the FD technique for the eight structural models defined in Fig. 2. The two thick black curves (4) correspond to results obtained for the detailed model of the site as given by Maurer *et al.* (1999) assuming the two bedrock structures. Curves (1) and (2) correspond to the simplified models with just one layer ($v_S = 222$ and 203 m s^{-1}) and curve (3) to the average structure with two layers for the soft sediments. (b) Comparison between H/V ratios of observed (thin grey lines) and synthetic noise generated with modal summation (black lines) with uncorrelated *SH* noise added to the signals. Both parts show application of the method based on the classical Fourier H/V method.

frequency–time analysis is given as a thin grey line in Fig. 10(a). These curves for the two methods are very similar, which supports the assumption made for the spectral content of the *SH* wavefield. It is possible to find a structural model for which the fundamental-mode Rayleigh wave (thick grey line in Fig. 10a) and the average H/V ratio from numerical simulations (thick black line) explain the observations. The example shown refers to observation point 2 in Fig. 1.

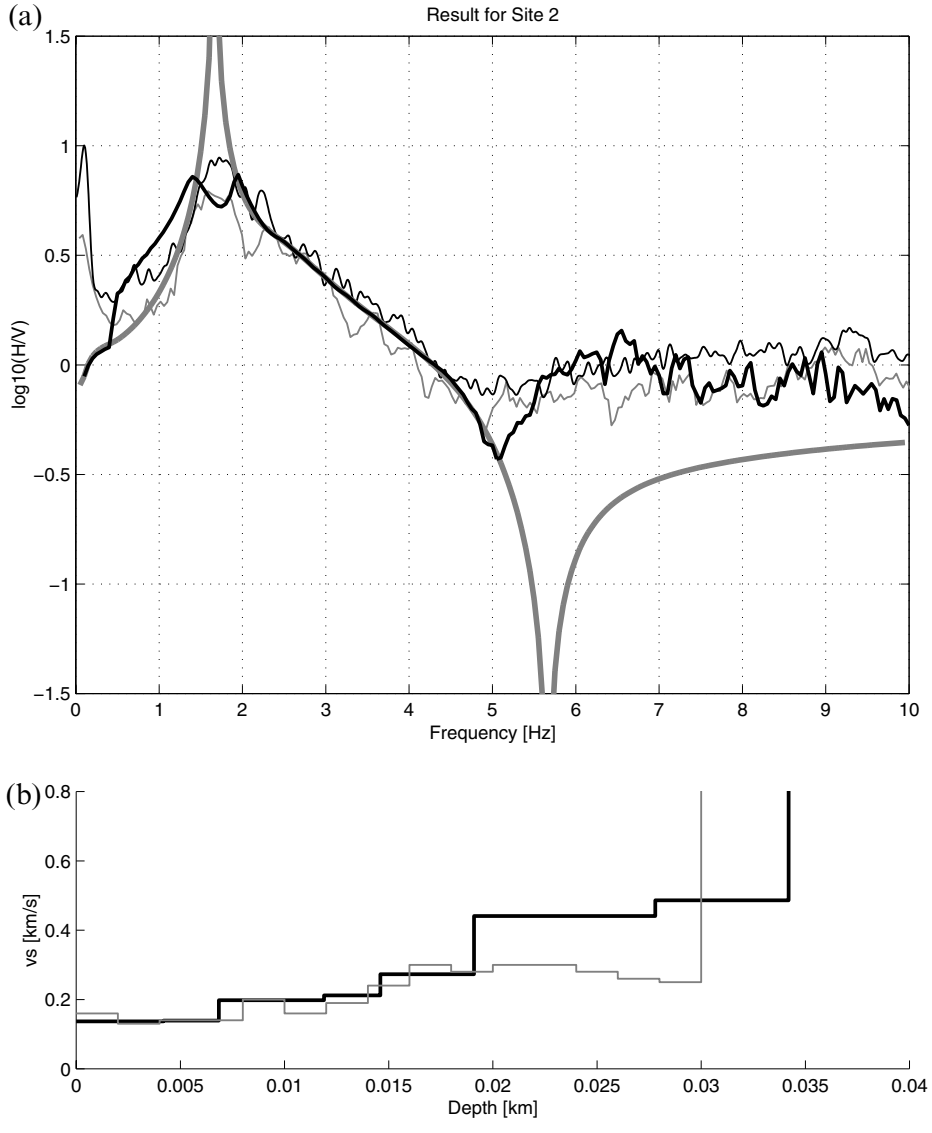

Figure 10. (a) Comparison between H/V ratios of observed noise (thin lines) and synthetic noise (thick black line) for the structural model shown in (b). The thin black line is the result from the classical polarization analysis in the frequency domain applied to the observed signals and corrected for *SH* waves. The thin grey line is obtained with the method based on the frequency–time analysis. The thick black line is the average H/V ratio over all distance ranges obtained with modal summation for the structure in (b). The thick grey line in the background is the ellipticity of the fundamental-mode Rayleigh wave for this structure. (b) Structural model obtained from the inversion of the observed H/V ratios (thick black line) compared to the model given by Maurer *et al.* (1999) (thin grey line).

The model in Fig. 10(b) (black curve) has been found by inverting for the structure so that the ellipticity of the fundamental-mode Rayleigh wave is best fitted to the observed H/V ratios in the frequency band between the fundamental frequency of resonance f_0 and the first minimum of the H/V ratios. Due to the non-linear nature of the forward problem, our solution of the inverse problem is based on a genetic algorithm. Genetic algorithms do not require an explicit starting model and are generally very robust and easy to adapt to a specific problem. For the inversion, the layer thickness and shear wave velocity of seven layers for the unconsolidated sediments and for one bedrock layer are selected as free parameters. The maximum depth of the sediments is limited to 35 m.

The H/V ratios from the inverted structure fit the observations well. They show a good agreement with the ellipticity of the fundamental mode, except at the fundamental frequency itself. Again the agreement at low frequencies for the ratio obtained with the frequency–time analysis is remarkable. For higher frequencies the agreement is better than for the eight initial models, as no further significant peaks appear.

For the first 18 m the inverted shear wave velocity structure is almost identical to the measured structure. Further down the structures start to differ because the details of the moraine layer and the properties of the bedrock cannot be resolved by the seismic surface-to-borehole transmission experiment. Therefore, the inverted model corresponds well to the measured velocity profile. Generally, in soft sediments the shear wave velocity increases with depth, so the inverted structure is quite likely. The inverted structural model is not a unique solution. This example demonstrates the possibility of inverting observed H/V ratios. Further tests will define the uncertainty of the inversion, and this will be the target of further research.

CONCLUSIONS

Stable parts of average H/V ratios have been identified that are independent of the source distance but sensitive to the detailed local structure. For our test site these parts are governed by the ellipticity of the fundamental-mode Rayleigh wave in the frequency band between the fundamental frequency of resonance of the unconsolidated sediments and the first minimum of the average H/V ratio. The ellipticity in this frequency band depends mostly on the S-wave velocity depth distribution of the unconsolidated sediments. This has been verified with two independent methods, modal summation and a finite difference technique. The ellipticity in this frequency band is given by the layering of the sediments. This observation is restricted to large contrasts between bedrock and sediments. The source distances and impedance contrast between sediments and bedrock have a large effect on the amplitude and frequency of the maximum H/V ratio. This uncertainty makes the frequency of the maximum ratio alone an uncertain parameter.

Our results are in contradiction to the results obtained by Nakamura (2000). Even if the variability of the H/V ratio at the peak is high due to differences in the P–SV-wave composition, no SH-wave resonance effect is needed to explain observed H/V ratios. The fundamental-mode Rayleigh wave is not the dominant wave type at this peak; rather, higher-mode Rayleigh waves are. They are also polarized at the fundamental frequency of resonance of the sediments, which can explain the peak of the H/V ratio. In the frequency range above the fundamental frequency of resonance of the unconsolidated sediments, fundamental-mode Rayleigh waves strongly dominate the wavefield. Nevertheless, we are not able to draw conclusions about the contribution of SH waves to the peak of observed H/V ratios. From a single station measurement of ambient vibrations it is not possible to distinguish SH waves from P–SV waves. Measurements of ambient vibrations on arrays of seismic stations could provide an answer to this question.

Two methods have been applied to compute average H/V ratios, the classical method in the frequency domain and a new method based on the frequency–time analysis, which allows one to locate P–SV wavelets in the time-series. A combination of the two methods can help to constrain the contribution of SH waves better. The advantage of the frequency–time method is the better detection of the minimum of the H/V ratio, whereas classical H/V ratios based on Fourier spectra are better for large H/V values close to the fundamental frequency of resonance of the unconsolidated sediments. At low frequencies, the H/V ratio obtained with the frequency–time analysis agrees well with the ellipticity of the fundamental-mode Rayleigh wave.

We invert the stable part in the average H/V ratio for the fine structure of the unconsolidated sediments using a genetic algorithm. On the assumption of equal spectral contents of SH waves and the radial component of P–SV waves, we retrieve a structure from single-site noise measurements that is almost identical to that derived from very expensive geophysical surveys. This method needs further tests in order to define the space of possible solutions better and to describe the limit of its applicability for structures with a small impedance contrast between sediments and bedrock.

The proposed method is relevant in earthquake engineering because it allows one to estimate shear wave velocities of the unconsolidated sediments at a low cost. Further studies at well-investigated test sites will help to improve the proposed method and to define the limits of its applicability.

ACKNOWLEDGMENTS

We thank G. F. Panza and the Seismology Group of Trieste University for the use of the spectral part of the Rayleigh waves program. The public domain driver for the genetic algorithm was developed by D. L. Carroll. We would like to thank R. Madariaga and two unknown reviewers for their contributions to improving this paper. ETH-Geophysics contribution No. 1152.

REFERENCES

Boore, D.M. & Brown, L.T., 1998. Comparing shear-wave velocity profiles from inversion of surface-wave phase velocities with downhole measurements: systematic differences between the CXW method and downhole measurements at six USC strong-motion sites, *Seism. Res. Lett,* **69,** 222–229.

Dravinski, M., Ding, G. & Wen, K.-L., 1996. Analysis of spectral ratios for estimating ground motion in deep basins, *Bull. seism. Soc. Am.,* **86,** 646–654.

Emmerich, H., 1989. 2-D wave propagation by a hybrid method, *Geophys. J. Int.,* **99,** 307–319.

Emmerich, H. & Korn, M., 1987. Incorporation of attenuation into time-domain computations of seismic wave fields, *Geophysics,* **52,** 1252–1264.

Fäh, D., 1992. A hybrid technique for the estimation of strong ground motion in sedimentary basis, *PhD thesis,* ETH, Zurich.

Fäh, D., Rüttener, E., Noack, T. & Kruspan, P., 1997. Microzonation of the city of Basel, *J. Seism.,* **1,** 87–102.

Florsch, N., Fäh, D., Suhadolc, P. & Panza, G.F., 1991. Complete synthetic seismograms for high frequency multimode SH-waves, *Pageoph,* **136,** 529–560.

Knopoff, L., 1964. A matrix method for elastic wave problems, *Bull. seism. Soc. Am.,* **54,** 431–438.

Lachet, C. & Bard, P.-Y., 1994. Numerical and Theoretical Investigations on the possibilities and limitations of Nakamura's technique, *J. Phys. Earth,* **42,** 377–397.

Lermo, J. & Chavez-Garcia, J., 1994. Are microtremors useful in site response evaluation?, *Bull. seism. Soc. Am.,* **84,** 1350–1364.

Levander, A.R., 1988. Fourth-order finite-difference P-SV seismograms, *Geophysics,* **53,** 1425–1436.

Maurer, H.R., Van der Veen, M., Giudici, J. & Springman, S., 1999. Determining elastic soil properties at small strains, *Proc. SAGEEP Mtng, Oakland, USA*, submitted.

Nakamura, Y., 1989. A method for dynamic characteristics estimation of subsurface using microtremor on the ground surface, *QR RTRI,* **30,** 25–33.

Nakamura, Y., 2000. Clear identification of fundamental idea of Nakamura's technique and its applications, *Proc. XII World Conf. Earthquake Engineering, New Zealand,* Paper no 2656.

Panza, G.F., 1985. Synthetic seismograms: the Rayleigh waves modal summation, *J. Geophys.,* **58,** 125–145.

Panza, G.F. & Suhadolc, P., 1987. Complete strong motion synthetics, in *Seismic Strong Motion Synthetics,* ed. Bolt, B. A, *Computational Techniques,* **4,** 153–204.

Schwab, F., 1970. Surface-wave dispersion computations: Knopoff's method, *Bull. seism. Soc. Am.,* **61,** 1491–1520.

Schwab, F., Nakanishi, K., Cuscito, M., Panza, G.F., Liang, G. & Frez, J., 1984. Surface-wave computations and the synthesis of theoretical seismograms at high frequencies, *Bull. seism. Soc. Am.,* **74,** 1555–1578.

Virieux, J., 1986. P-SV wave propagation in heterogeneous media: velocity-stress finite-difference method, *Geophysics,* **51,** 889–901.